Published in final edited form as:
Hum Brain Mapp. 2009 April ; 30(4): 1257–1270. doi:10.1002/hbm.20591.

Alcohol Dose Effects on Brain Circuits During Simulated Driving: An fMRI Study

Shashwath A. Meda[1,*], **Vince D. Calhoun**[1,2,3,4,5], **Robert S. Astur**[1,2], **Beth M. Turner**[1], **Kathryn Ruopp**, and **Godfrey D. Pearlson**[1,2,3]

[1] Olin Neuropsychiatry Research Center, Institute of Living at Hartford Hospital, Hartford, Connecticut [2] Department of Psychiatry, Yale University School of Medicine, New Haven, Connecticut [3] Department of Psychiatry, Johns Hopkins University, Baltimore, Maryland [4] The MIND research network, Albuquerque, New Mexico [5] Department of Electrical and Computer Engineering, University of New Mexico, Albuquerque, New Mexico

Abstract

Driving while intoxicated remains a major public health hazard. Driving is a complex task involving simultaneous recruitment of multiple cognitive functions. The investigators studied the neural substrates of driving and their response to different blood alcohol concentrations (BACs), using functional magnetic resonance imaging (fMRI) and a virtual reality driving simulator. We used independent component analysis (ICA) to isolate spatially independent and temporally correlated driving-related brain circuits in 40 healthy, adult moderate social drinkers. Each subject received three individualized, separate single-blind doses of beverage alcohol to produce BACs of 0.05% (moderate), 0.10% (high), or 0% (placebo). 3 T fMRI scanning and continuous behavioral measurement occurred during simulated driving. Brain function was assessed and compared using both ICA and a conventional general linear model (GLM) analysis. ICA results replicated and significantly extended our previous 1.5T study (Calhoun et al. [2004a]: Neuropsychopharmacology 29:2097–2017). GLM analysis revealed significant dose-related functional differences, complementing ICA data. Driving behaviors including opposite white line crossings and mean speed independently demonstrated significant dose-dependent changes. Behavior-based factors also predicted a frontal-basal-temporal circuit to be functionally impaired with alcohol dosage across baseline scaled, good versus poorly performing drivers. We report neural correlates of driving behavior and found dose-related spatio-temporal disruptions in critical driving-associated regions including the superior, middle and orbito frontal gyri, anterior cingulate, primary/supplementary motor areas, basal ganglia, and cerebellum. Overall, results suggest that alcohol (especially at high doses) causes significant impairment of both driving behavior and brain functionality related to motor planning and control, goal directedness, error monitoring, and memory.

Keywords

ICA; virtual reality; DWI; driving behavior; functional imaging

*Correspondence to: Shashwath A. Meda, Olin Neuropsychiatry Research Center/IOL, 200 Retreat Avenue, Hartford, CT 06106, USA. E-mail: smeda01@harthosp.org.

Published online in Wiley InterScience (www.interscience.wiley.com).

INTRODUCTION

Impaired driving under the influence of alcohol is a major public hazard in the United States. Alcohol-related crashes are the primary source of traffic fatalities, as evidenced by almost 17,000 deaths (nearly 40%) and 250,000 injuries in the year 2004 alone (NHTSA safety facts, 2004). Recently, several studies have illustrated the potential usefulness of simulated driving environments to evaluate brain function in combination with various pharmacologic challenges [Arnedt et al., 2001; Calhoun et al., 2004b; Deery and Fildes, 1999; Linnoila et al., 1973; Rimm et al., 1982; Verster et al., 2002]. However, to our knowledge, we are the first to have used functional magnetic resonance imaging (fMRI) to probe temporal brain dynamics while driving under the influence of alcohol [Calhoun et al., 2002, 2004a, 2005]. Studying the effects of alcohol on a multifaceted functional paradigm such as driving a motor vehicle is potentially complex. However, virtual reality (VR) or simulated environments in conjunction with fMRI, as used in our study, can provide better insights on the effect of drugs on complex brain functions and behavior.

Alcohol has significant, dose-dependent effects on neuropsychological processes including short term memory [Rosen and Lee, 1976; Tarter et al., 1991], sustained and divided attention [Lamb and Robertson, 1987; Moskowitz and Sharma, 1974] and motor coordination [Groeger, 2001 (Willingham's COBALT model); Tarter and Jones, 1971], all of which are components of driving [Groeger, 2001]. Event related potential (ERP) and other psychophysiological measures suggests slower information processing due to alcohol intoxication [Colrain et al., 1993; Krull et al., 1993]. Several studies have examined the neural substrates of sober driving using fMRI or Positron emission tomography (PET) [Calhoun et al., 2002; Graydon et al., 2004; Jeong et al., 2006; Spiers and Maguire, 2007; Uchiyama et al., 2003; Walter et al., 2001]. In accord with our previous studies [Calhoun et al., 2002, 2004a], this current study examined neural networks associated with driving and effects of alcohol intoxication. However, in the present study, rather than a commercially available software program we used a custom built virtual reality (VR) environment to increase realism and ecological validity. As part of the VR setup, we used a scanner-compatible steering wheel and foot-operated brake and gas pedals rather than a modified hand-held videogame controller, to closely mimic a real time driving scenario. Further, in the current study we scanned more participants at a higher field strength (3 T) to increase our power and to extend our results across systems. The new environment also automatically records behavioral measures (whereas in previous studies we used double rated measures derived from digital recordings of the sessions).

In analyzing data, independent component analysis (ICA) utilizes a data driven approach to effectively disassociate multiple activation networks involved in complex tasks with little or no assumptions about the temporal dynamics of the data. On the other hand, a GLM (conventional SPM analysis) based analysis uses a mass univariate multiregression approach to explore signal correlations between a prespecified paradigm design and acquired data time courses across the whole brain. In the present study we used both ICA and a conventional GLM analysis, as discussed by Calhoun et al., 2004a.

We had several aims for the present study: (1) To replicate and extend our previous results [Calhoun et al., 2002, 2004a] in delineating the underlying networks involved while driving; (2) To identify dose-related disruptions in component-specific time courses in additional driving related circuits; and (3) To identify individual behavioral and associated neural network changes while driving intoxicated.

More specifically, because of the higher field strength and increased number of subjects in the current study, we expected to improve power and therefore delineate additional task related networks involved while driving an automobile. We also sought to demonstrate alcohol

intoxication effects in additional circuits such as the cerebellum which was associated with a behavioral measure (speed) but did not show a main effect of alcohol in our previous study. Also, since we now employed an extended driving epoch in our design (details presented later) we expected to detect significant alcohol-related changes with the conventional regression analysis as well.

EXPERIMENTS AND METHODS

Subjects

The study included 40, healthy, right-handed men ($N = 20$) and women ($N = 20$), with a mean age of 24.75 ± 4.7 years. Potential participants were screened to eliminate those with any neurological disorder or DSM IV-TR Axis I psychiatric disorder including a history of substance abuse [Janca et al., 1994]. At each visit, participants underwent a urine drug screen to test for drugs and pregnancy in women. All participants were nonsmokers, had good visual acuity without correction, valid driver's licenses, good driving records assessed by self report, and were light or moderate users of alcohol (1–4 alcohol consumption sessions/week and 1–8 drinks/session; average consumption/month, nine times with an average of four drinks per occasion). Participants were trained for 10 min. on the simulated driving paradigm. To avoid interfering with the alcohol absorption, they were requested to eat only a light meal (avoiding fatty foods) on the morning of each study and to avoid consuming alcohol for 24 h prior to each study day.

Each participant received an individualized dose of beverage alcohol calculated based on body weight and sex following a published algorithm [Kapur, 1989] in a blinded, randomized trial. Doses were designed to achieve a moderate (blood alcohol concentration (BAC), 0.05%) or a high (BAC, 0.10%) effect. All drinks, including placebo, were in identical beverage containers wrapped with an alcohol soaked cloth and with an additional small amount of alcohol on the surface of the drink to help disguise the contents [Hammersley et al., 1992]. All drinks were made with orange or cranberry juice to constant volume of 350 ml. BAC's were measured before drinking to assure participants were not already under the influence and at regular intervals after each scan session using a hand-held breathalyzer (Intoximeters) calibrated regularly using an ethanol breath standard sample dispensing device. All subjects gave written informed consent prior to participation in the study, which was approved by the Hartford Hospital Institutional Review Board.

Procedures

Participants were asked to pace their consumption over 10 min. BAC's were tested after 5 and 10 min of alcohol consumption. On average, participants were brought into the MRI 15 min after consumption was completed. The average BAC's for the moderate dose when entering the scanner was 0.039 ± 0.014 and when exiting was 0.032 ± 0.011. Similarly for the high dose average BAC's when entering the scanner was 0.071 ± 0.017 and when exiting was 0.087 ± 0.013. After their MRI, participants were brought to a room where they were able to watch movies, search the internet, or sleep. Participants were also provided food of their choice and plenty of water. Study doctors determined when it was OK for participants to leave (BAC of 0.05 via cab or friend, BAC of 0.00 on own) and signed participants out. All subjects were able to successfully complete the consumption of both moderate and high doses of alcohol without feeling nauseous.

Equipment Design and Setup

The driving simulator used custom built in-house software. The hardware setup (Fig. 1) was designed to mimic a realistic driving experience and capture real time aspects of driving behavior, with a steering wheel, accelerator, and brake pedals. All ferromagnetic components

in this hardware were replaced with nonferromagnetic (plastic or copper-beryllium) parts. The controller itself was connected to a computer outside the scanner room through a waveguide in the wall. An LCD projector (SHARP XG-P25X) outside the scanner room and behind the scanner projected through a second waveguide to a translucent screen, which the subjects saw via a mirror attached to the head coil of the 3 T MRI scanner (Allegra; Siemens, Erlangen, Germany). The screen subtended approximately a 25° field of view (FOV) that provided the subject with a straight line of sight.

The functional paradigm was blocked (Shown in Fig. 2) and each run consisted of three epochs, fixation (30 s), drive (90 s), and observe (60 s), each repeated three times and ending with a fixation epoch. During the fixation phase, the subject was instructed to focus on a + sign. During the driving block, the participant was asked to drive the car normally and safely, abide by all conventional traffic rules (posted speed limit [40 mph], stop signs, yielding for pedestrians, staying in the right lane except to pass). During the observe phase, the subject passively viewed a simulated driving scene. Each run was repeated three times (separately) to increase the signal to noise ratio (SNR).

Data Acquisition

Driving behavior—Continuous behavioral variables including, passenger side white line crossings, median/yellow line crossings, opposite side white line crossings, crashes, speed, and steering weave were recorded during the driving phase of the experiment. At the end of each run, an overall summary score for each behavior was created for every subject. Performance was averaged across the three driving epochs and the three scan runs.

Imaging—Functional data were acquired on a Siemens Allegra 3 T scanner at the Olin Neuropsychiatry Research Center at the Institute of Living using an echoplanar sequence using the following imaging parameters; repeat time (TR) = 1,500 ms, echo time (TE) = 27 ms, field of view (FOV) = 22 cm, flip angle = 70°, acquisition matrix = 64 × 64, voxel size = 3.44 × 3.44, slice thickness = 5 mm, number of slices = 29, ascending acquisition (sequential). The scanner was equipped with 40 mT/m gradients and a standard quadrature head coil. To achieve longitudinal equilibrium, six dummy scans were performed at the beginning and discarded prior to analysis. Scanning was automatically triggered by the paradigm.

Data Processing

Driving behavior—Behavioral variables were investigated for dosage related responses. All measures were also screened for any major outliers before conducting any statistical analysis. A one-way repeated measures ANOVA design was created to look at the effect of alcohol on each behavioral variable separately.

Image preprocessing—All images were preprocessed using the SPM2 Software (http://www.fil.ion.ucl.ac.uk/spm/software/spm2/). Motion correction was achieved using INRIAlign [Freire and Mangin, 2001; Freire et al., 2002] to compensate for movement in the fMRI time series images. Each subjects' movement parameters were screened to ensure absence of excessive head motion. Motion corrected images were then spatially normalized to Montreal Neurological Institute (MNI) space by matching them to the standardized EPI template image in SPM. After spatial normalization, images were spatially smoothed with an 8 mm isotropic Gaussian kernel. Both GLM and ICA operated on the same set of preprocessed images.

fMRI and ETOH (Ethyl Alcohol or Ethanol)

Conventional GLM (SPM) analysis—As part of the first level (subject level) design, for each subject and dose, regressors were created for the drive and observe conditions. Regressors

were then convolved with the standard hemodynamic response function (hrf) available in SPM2 and a multiple regression was performed. Contrasts were then generated for the following conditions: (1) Drive alone (Drive vs. Fixation); (2) Observe alone (Observe vs. Fixation); and (3) Drive > Observe. A second level (group level) random-effect (RFX) analysis was then carried out to measure the effect of dose response on all three contrasts separately using a repeated measure ANOVA incorporated through the GLM framework. At the group level bi-directional one tailed contrasts were created to look for activation differences between the following (1) placebo and moderate dose, (2) placebo and high dose, (3) moderate dose and high dose. The resulting set of voxels from each contrast represents a statistical parametric map of the t-statistic (SPM-t). SPM-t maps comprised of results of statistical tests on each voxel, thresholded at $P < 0.05$ and corrected for multiple comparisons using the false discovery rate [FDR; Genovese et al., 2002].

To visualize dosage-related differences, the SPM coordinates and significant voxels were superimposed onto SPM2's spatially normalized template brain. Voxel coordinates are reported in Montreal Neurological Institute (MNI) space. Corresponding Talairach labels (Brodmann areas) are reported after converting MNI coordinates to the standard space of Talairach and Tournoux [Talairach and Tournoux, 1988] using a MATLAB program written by Matthew Brett (MRC Cognition and Brain Sciences Unit, Cambridge, England). Once converted, the Talairach coordinates were entered into the Talairach Daemon [Lancaster et al., 2000] for result localization.

ICA analysis—To reveal spatiotemporal associations we conducted an analysis using a group ICA algorithm [Calhoun et al., 2001]. The ICA methods are available as a toolbox (GIFT v1.3c) implemented in Matlab (http://icatb.sourceforge.com). ICA operated on the preprocessed images mentioned above. To briefly review the specifics of this approach, data from all subjects were pooled into a single ICA analysis, followed by a back reconstruction of single subject time courses and spatial maps from the raw data. Data were reduced through two principal component analysis (PCA) stages [Calhoun et al., 2001]. Following this 24 mutually independent component were estimated by ICA using the infomax approach [Bell and Sejnowski, 1995], the number of components was determined using the minimum length description (MDL) criteria adjusted to account for correlated samples [Li et al., 2007]. Time courses and spatial maps were then reconstructed for each subject. The resulting single subject time course amplitudes were scaled to z-scores using the raw data to reflect normalized values. Further, the time courses were parameterized using multiple regression to provide association estimates (beta weights) between component time courses and the same experimental design used in the GLM that modeled the drive and observe conditions.

Before conducting statistical analysis on the ICA time course data, the regression fit values for all three runs were averaged together (an apriori analysis revealed no significant "within-run" effect across components). Finally, we arrived with 14 components of interest and 40 subjects with 3 dosages each, thus yielding a total of 120 time courses per component. We tested for dose-related changes in each component, regardless of behavior.

Dose-related changes were statistically assessed using a two-way repeated measures ANOVA design in SPSS v15.0 on all 14 components. The analysis investigated two main effects (condition [drive and observe] and dosage [high, moderate, placebo]) and an interaction effect (condition × dosage) on the association estimates obtained from ICA across all 14 components. We were primarily interested in significant interaction effects to determine the effect of alcohol on driving component time courses.

Driving Behavior, fMRI, and Etoh

Further, to identify neural correlates of behavior, we divided subjects into good and poor performing drivers using their behavior from the placebo and high doses only. To do this, all individual behavioral variables were corrected for subject's baseline performance (raw driving scores from the placebo condition subtracted from the high dose condition). Corrected scores from all variables were then pooled into a principal component analysis (PCA; using varimax rotation) in SPSS v15.0 (http://www.spss.com/spss/) to generate factors that predicted overall behavioral performance. Only factors yielding a principle Eigenvalue score >1 were retained for further analysis. Factor coefficients scores were estimated using the Anderson-Rubin method, thus ensuring orthogonality and normality of the estimated factors. Further, a mean-split of each factor variable was used separately to divide the original sample into two groups (good and poor performing drivers). A 2 by 3 repeated measures ANOVA was designed to look at any significant interaction between driver-group fMRI responses and alcohol dosage. Interactions were investigated only in components that demonstrated a significant ICA related fMRI change with alcohol (details in later section).

RESULTS

Driving Behavior

Behavioral analysis used only a subset of the original sample (37/40), three subjects were classified as outliers on behavior and were not included in the analysis. A main effect analysis of behavioral data across alcohol dosage (Placebo, moderate and high) revealed that opposite white line crossings ($P = 0.009$; df = 35) and mean speed ($P = 0.03$; df = 35) were significantly different and demonstrated a dose-related linear response (Fig. 3). Other behavioral variables, although not significantly affected by alcohol dose, demonstrated a similar linear trend, associating higher alcohol dose with increased crashes, steering weave and more frequent crossing of passenger side white lines (Fig. 3).

fMRI and Etoh

GLM results—All 40 subjects were within the acceptable motion criteria set apriori (less than 3 mm of translational and 2° of rotational motion), and were thus included in the analysis. Random effect analysis did not reveal any significant dose-related changes in brain functionality for the drive alone (active driving) or observe alone (passive driving) contrasts. However, when we examined dose-related changes in activation patterns using the drive relative to observe contrast (active driving versus passive driving), multiple cortical regions displayed significantly less activation in the high dose relative to the placebo condition (Fig. 4a,b). The functional differences between the placebo and moderate dose conditions (albeit not significant) demonstrated a trend in the same direction. Regions along with their MNI coordinates and Brodmann areas are listed in Table I. As seen from the table, multiple regions from the GLM analysis overlapped with the ICA components. In addition, the GLM analysis revealed significant changes in regions, including the amygdala and hippocampus/parahippocampus that did not emerge significant in the ICA analysis. GLM failed to capture regional activation in cerebellum and motor. In addition, GLM was able to capture only a part of the default mode network, which has been defined as a baseline condition of brain function [Raichle et al., 2001]

GLM results revealed five major regions (Fig. 4a): R parahippocampus-hippocampus-amygdala (yellow circle), R inferior frontal (pink circle), bilateral medial-superior frontal gyri/dorsolateral prefrontal cortex (Green and Blue circles), and precuneus (orange circle) that demonstrated a significant dose-related response during the drive versus observe condition. We plotted effect sizes in each of these regions to investigate signal change as a function of

dosage. As seen from Figure 5, GLM results revealed a linear fMRI signal pattern ordered in all five regions as sober > moderate > high.

ICA Results

Overall, using ICA we identified 14 total driving related components of interest. In addition to finding all 7 component specific regions from our previous paper, we found several additional regions/components (frontal, inferior temporal, middle temporal) which showed task-related changes. We also observed that some components identified our previous study (e.g. cerebellar and visual) were now extracted as separate components. The two-way ANOVA comparison on the 14 driving related components revealed 5 of the 14 networks [Fig. 6; color coding scheme used here is not similar to the one described by Calhoun et al., 2004a] to have a significant alcohol related change in functional synchrony including cerebellar (pink component), orbito-frontal/anterior cingulate (red component), medial frontal-parietal-posterior cingulate (resting state network; orange component), fronto-basal-temporal (green component), and primary-supplementary motor (blue component). The regions shown in Figure 3 were thresholded at $P = 0.05$ (FDR corrected). The corresponding MNI coordinates of the regions, along with their hypothesized functionality, are listed in Table II. Other driving-related circuits that were identified by ICA but did not show a significant alcohol-related change included the bilateral medial-inferior frontal gyrus, the inferior frontal-anterior and posterior cingulate cortex, inferior temporal/hippocampus, bilateral superior occipital, right inferior occipital/cerebellum, and posterior cerebellum (split into three components).

Driving Behavior, fMRI, and Etoh

To investigate the neural correlates of behavior, we used PCA along with varimax rotation to generate surrogate behavioral factors for each subject. The top two, PCA factors (Eigenvalues of 1.91 and 1.85), cumulatively accounted for 63% of the total behavioral variance (Table III). Behavioral measures of driver speed, steering weave, and passenger side white line crossings were primarily loaded (positively) on factor 1 (32% of total variance). Factor 2 (31% of total variance) was largely influenced (positively) by yellow/median line crossings, opposite white line crossings, and collisions. Factor 1 and factor 2 were highly uncorrelated. As revealed by a one-sample KS statistic, the two factors did not significantly differ from a normal distribution. This allowed us to separate the initial sample into two groups based on each factor separately using a mean split. On investigation of significant interaction between driver groups and alcohol dosage, poorer performing subjects based on behavior factor 1 demonstrated a significant dose-dependent change ($P = 0.04$; df = 35) in fMRI signal in the fronto-basal (green) component. Similarly, factor 2 demonstrated dose-related fMRI response change (albeit insignificant) for the resting state ($P = 0.15$; df = 35; orange) and motor ($P = 0.12$; df = 35; blue) networks.

DISCUSSION

In this study we explored the neural substrates of driving and addressed the overarching question of how alcohol impacts these driving networks using both imaging and behavioral measures. Driving is a dynamic task that requires a complex interplay between multiple cognitive domains. We therefore approached this analysis in a pluralistic manner using two complementary techniques, ICA and GLM, to effectively address our hypotheses.

We employed a novel custom built naturalistic driving setup to capture the internal and external aspects of driving psychology. External considerations include activities such as vehicle manipulation, road conditions, etc. The internal aspect of driving refers to the drivers' sensation, perception, verbalizations, thoughts decisions and emotions (http://www.soc.hawaii.edu/|leonj/|leonj/|leonpsy/|traffic/|tpintro.html). In contrast to a

behavioral study, which would mostly capture the variance due to the external aspects of driving, an fMRI experiment combined with VR or simulation can obtain information on both the internal and external aspects of driving. Compared to earlier studies conducted by our group, the present study used the following: (1) a larger sample size, (2) a higher field strength MR scanner, (3) custom built VR software that was automated to capture continuous driving related behavioral measures, (4) a modified design paradigm with an extended driving epoch, and (5) a different ICA and behavioral approach to analyze group data. Also, differently than our previous analysis [Calhoun et al., 2004a], which used a fixed average spatial ICA, the current study used data from the entire pool of subjects under all dosage conditions to estimate maximally independent components, thereby not biasing the results to the placebo condition alone. Using this approach we were able to replicate our previous results [Calhoun et al., 2004a] and extend the findings to identify twice as many driving related components.

Since alcohol is known to have vasoactive properties that may potentially confound BOLD fMRI signal [Levin et al., 1998; Seifritz et al., 2000] we performed an additional analysis using data from only the placebo condition to validate our methodology and determine if any new networks emerged as a result of alcohol ingestion. In this analysis of sober data, we were able to replicate all driving circuits as obtained for the pooled analysis, indicating that all networks that emerged in our study were evident during the sober state also. Although previous literature indicates that alcohol might affect the configuration (intra-connectivity) of networks in the absence of any dose-related magnitude difference [Paulus et al., 2006], data from our study suggest that the spatial preconfiguration of sober driving related networks was affected only slightly despite significant dose-dependent magnitude changes due to alcohol.

In our previous study, only two circuits (orbito-frontal and primary-supplementary motor) demonstrated significant dose-related responses [least activation occurring during the highest dose; Calhoun et al., 2004a], which correlated behaviorally with error detection and motor functionality. Overall, comparing the seven components identified by Calhoun et al., 2004a to similar regions found in the present study, we found them to be in good agreement both spatially and temporally. In line with our last study we found a significant alcohol related effect in the anterior cingulate/orbito-frontal circuit, which can be associated with error monitoring and span of attention [Calhoun et al., 2004a; Groeger, 2001; Spiers and Maguire, 2007.]. However, functionally, the greatest effect of alcohol dosage was found in the cerebellum, the primary-supplementary motor area and in the default mode network (Table II). The significant emergence of the cerebellum network in this study was consistent with our hypothesis but however unlike our results in Calhoun et al., 2004a, this network was not associated with any behavioral measure. Losses of gross and fine motor control are behavioral features of alcohol impairment [Tarter and Jones, 1971] and the motor and cerebellar regions identified are consistent with this, and with prior studies [see review of Oscar-Berman and Marinković, 2007). However, it may be important to note that the GLM analysis was not sensitive enough to be able to capture any dose-related fMRI changes in the above motor related components. This could perhaps be due to a passive recruitment of these regions [involved in nonconscious motor processing; Groeger, 2001 (Willingham's COBALT model)] during the observe phase of the experiment.

The default mode network has repeatedly exhibited significant functional connectivity across a wide variety of tasks and during a conscious inactive state. This circuit is associated with a baseline or "idling" brain condition and often demonstrates a decreased fMRI signal during performance of a variety of task stimuli [Fox and Raichle, 2007; Raichle et al., 2001]. Our findings are consistent with these prior reports (see time course data in Fig. 6) and also demonstrate that alcohol might have an impact on this network. Although the exact role of the default mode network is unknown, it has been implicated in attending to external and internal stimuli [Gusnard and Raichle, 2001; Gusnard et al., 2001; Raichle et al., 2001] as well as self-

referential and reflective activity [Greicius and Menon, 2004; Gusnard et al., 2001; Raichle et al., 2001] that includes episodic memory retrieval, inner speech, mental images, emotions, and planning future events [Fransson, 2005; Greicius and Menon, 2004]. Contrary to our last study, this network now demonstrated a significant main effect of alcohol thus suggesting that the fronto-parietal attentional control framework is modulated by alcohol during driving.

Although we did not detect the fronto-basal ganglia-temporal network in our previous ICA analyses, this component showed a significant alcohol related effect in the present study. This network is of interest as it overlaps most consistently with our GLM findings and is associated with complex cognitive tasks relevant to driving. The fronto-basal ganglia loop is often associated with executive, attentional control and goal directed responses [Benke et al., 2003; Dunnett et al., 2005; Hollerman et al., 2000; Levy and Czernecki, 2006]. The fronto-temporal network is likely to be involved in regulation of both working memory and attention [Aalto et al., 2005] and is especially sensitive to alcohol (Oscar-Berman and Marinković, 2007). Results from studies that have investigated driving abilities in subjects with fronto-temporal deficits often report inappropriate driving behavior [De Simone et al., 2007; Kamimura et al., 2005].

In contrast to our previous study [Calhoun et al., 2004a], but consistent with our present hypothesis, GLM with additional subjects in the current investigation was sensitive enough to reveal multiple regions that demonstrated a dose-dependent alcohol response. Further, GLM results overlapped in part with those of the ICA analysis and in addition captured dose-related responses in hippocampus and amygdala (Figs. 4 and 5). This illustrates the complementary nature of GLM and ICA analyses, where each contributes toward analyzing a complex functional task such as driving. As predicted, at the whole brain level, SPM analysis revealed a linear functional-dose response with alcohol causing decreased functional activity at both the moderate and high doses.

A decrease in the fMRI amplitude of the fronto-basal component with increased alcohol intoxication was related to higher speed, steering weave, and passenger white line errors. Also, a similar association (although not significant) was found in the medial frontal-parietal-cingulate (default mode) and motor networks that correlated with vehicle manipulation errors (crashes, median, and opposite white line errors). The latter association might not have been significant, perhaps due to the naturalistic nature (mimicking real time on-road scenarios) of the driving paradigm employed in our study, which allowed for a low number of such infrequent errors (crashes and opposite white line crossings). This suggests that marked impairment of behavior and functionality occur under the influence of alcohol relating to action/motor planning and higher cognitive judgments.

Our functional results correspond well with Willingham's COBALT model of motor control [illustrated in Groeger, 2001] in driving. In the COBALT model, the dorsolateral prefrontal cortex (part of the fronto-basal-temporal component in our study) is implicated in the strategic part of motor control, that which responds to novel, unfamiliar, or difficult tasks requiring conscious and controlled monitoring. In a later stage of processing, perceptual motor integration occurs through the posterior parietal lobe and premotor cortex (RSN and primary/supplementary motor networks; orange and blue circuits in Fig. 6), which leads to motor sequencing [performed by the supplementary motor areas and basal ganglia (parts of the primary/supplementary motor and fronto-basal-temporal networks)]. With reference to the above prediction model, our imaging results suggest that alcohol might have significant functional effects on both the conscious and non-conscious domains of motor control while automobile driving.

Even though we were able to derive and assess effects of alcohol on the temporal dynamics of several neural networks involved in driving and their associated behavior, our present paradigm design (blocked) prevents us from conducting and analyzing the data on a much finer temporal scale [Spiers and Maguire, 2007]. Also, it might be interesting for future studies to investigate the effect of gender on driving function/behavior with alcohol dosage.

Overall, results demonstrated the motor planning/goal direction (fronto-basal ganglia) system that correlated with driving speed, passenger white line errors and steering-related weaving to be significantly impaired with alcohol. Also, the default mode and primary motor systems were associated (although not significant) with crashes and line crossing errors in a dose-dependent manner. Further, in comparison to our findings from Calhoun et al., 2004a, our current data suggest that in addition to the anterior cingulate/OF and cerebellar regions, attention deficits for motor functioning observed in alcohol intoxication may also be modulated by regions in the resting state and the fronto-basal-temporal networks.

CONCLUSION

In summary, we replicated and significantly extended our earlier fMRI results revealing different activation dynamics for multiple regions during a simulated driving task. We used two complementary image analysis techniques to investigate alcohol-related changes in temporal dynamics of the driving circuitry at two dosage levels compared to placebo. We report five crucial networks including orbito-frontal/anterior cingulate, fronto-temporal, primary/secondary motor, cerebellar, and the resting state networks as being modulated by alcohol in a dose-related manner. Additionally, a conventional GLM analysis captured a significant dose-dependent response in areas including the amygdala and parahippocampus. Further, we found consistent behavioral changes while driving intoxicated supporting our imaging results. Our results demonstrated that speed and white line crossing errors mediated the fronto-basal ganglia-temporal (green) component involvement across alcohol dosages. Overall, our findings might imply a significant impairment in attention, cognitive, goal direction, motor planning and emotional/working memory related functional capabilities while driving under the influence of alcohol.

Acknowledgments

Contract grant sponsor: National Institutes of Health; Contract grant numbers: 1 R01 EB 000840-015 R01 AA015615-02

References

Aalto S, Bruck A, Laine M, Nagren K, Rinne JO. Frontal and temporal dopamine release during working memory and attention tasks in healthy humans: A positron emission tomography study using the high-affinity dopamine D2 receptor ligand [11C]FLB 457. J Neurosci 2005;25:2471–2477. [PubMed: 15758155]

Arnedt JT, Wilde GJ, Munt PW, MacLean AW. How do prolonged wakefulness and alcohol compare in the decrements they produce on a simulated driving task? Accid Anal Prev 2001;33:337–344. [PubMed: 11235795]

Bell AJ, Sejnowski TJ. An information-maximization approach to blind separation and blind deconvolution. Neural Comput 1995;7:1129–1159. [PubMed: 7584893]

Benke T, Delazer M, Bartha L, Auer A. Basal ganglia lesions and the theory of fronto-subcortical loops: Neuropsychological findings in two patients with left caudate lesions. Neurocase 2003;9:70–85. [PubMed: 16210227]

Calhoun VD, Adali T, Pearlson GD, Pekar JJ. A method for making group inferences from functional MRI data using independent component analysis. Hum Brain Mapp 2001;14:140–151. [PubMed: 11559959]

Calhoun VD, Pekar JJ, McGinty VB, Adali T, Watson TD, Pearlson GD. Different activation dynamics in multiple neural systems during simulated driving. Hum Brain Mapp 2002;16:158–167. [PubMed: 12112769]

Calhoun VD, Pekar JJ, Pearlson GD. Alcohol intoxication effects on simulated driving: Exploring alcohol-dose effects on brain activation using functional MRI. Neuropsychopharmacology 2004a; 29:2097–3017. [PubMed: 15316570]

Calhoun VD, Altschul D, McGinty V, Shih R, Scott D, Sears E, Pearlson GD. Alcohol intoxication effects on visual perception: An fMRI study. Hum Brain Mapp 2004b;21:15–26. [PubMed: 14689506]

Calhoun VD, Carvalho K, Astur R, Pearlson GD. Using virtual reality to study alcohol intoxication effects on the neural correlates of simulated driving. Appl Psychophysiol Biofeedback 2005;30:285–306. [PubMed: 16167192]

Colrain IM, Taylor J, McLean S, Buttery R, Wise G, Montgomery I. Dose dependent effects of alcohol on visual evoked potentials. Psychopharmacology (Berl) 1993;112:383–388. [PubMed: 7871046]

De Simone V, Kaplan L, Patronas N, Wassermann EM, Grafman J. Driving abilities in frontotemporal dementia patients. Dement Geriatr Cogn Disord 2007;23:1–7. [PubMed: 17047327]

Deery HA, Fildes BN. Young novice driver subtypes: Relationship to high-risk behavior, traffic accident record, and simulator driving performance. Hum Factors 1999;41:628–643. [PubMed: 10774133]

Dunnett SB, Meldrum A, Muir JL. Frontal-striatal disconnection disrupts cognitive performance of the frontal-type in the rat. Neuroscience 2005;135:1055–1065. [PubMed: 16165288]

Fox MD, Raichle ME. Spontaneous fluctuations in brain activity observed with functional magnetic resonance imaging. Nat Rev Neurosci 2007;8:700–711. [PubMed: 17704812]

Fransson P. Spontaneous low-frequency BOLD signal fluctuations: An fMRI investigation of the resting-state default mode of brain function hypothesis. Hum Brain Mapp 2005;26:15–29. [PubMed: 15852468]

Freire L, Mangin JF. Motion correction algorithms may create spurious brain activations in the absence of subject motion. Neuroimage 2001;14:709–722. [PubMed: 11506543]

Freire L, Roche A, Mangin JF. What is the best similarity measure for motion correction in fMRI time series? IEEE Trans Med Imaging 2002;21:470–484. [PubMed: 12071618]

Genovese CR, Lazar NA, Nichols T. Thresholding of statistical maps in functional neuroimaging using the false discovery rate. Neuroimage 2002;15:870–878. [PubMed: 11906227]

Greicius MD, Menon V. Default-mode activity during a passive sensory task: Uncoupled from deactivation but impacting activation. J Cogn Neurosci 2004;16:1484–1492. [PubMed: 15601513]

Graydon FX, Young RA, Tdss MD, Tdss B, Genik RJ II, Posse S, Hsieh L, Green CC. Visual event detection during simulated driving: Identifying the neural correlates with functional neuroimaging. Transp Res Part F Traffic Psychol Behav 2004;7:271.

Groeger, JA. Understanding Driving: Applying Cognitive Psychology to a Complex Everyday Task. New York: Psychology Press; 2001.

Gusnard DA, Raichle ME. Searching for a baseline: Functional imaging and the resting human brain. Nat Rev Neurosci 2001;2:685–694. [PubMed: 11584306]

Gusnard DA, Akbudak E, Shulman GL, Raichle ME. Medial prefrontal cortex and self-referential mental activity: Relation to a default mode of brain function. Proc Natl Acad Sci USA 2001;98:4259–4264. [PubMed: 11259662]

Hammersley R, Finnigan F, Millar K. Alcohol placebos: You can only fool some of the people all of the time. Br J Addict 1992;87:1477–1480. [PubMed: 1422109]

Hollerman JR, Tremblay L, Schultz W. Involvement of basal ganglia and orbitofrontal cortex in goal-directed behavior. Prog Brain Res 2000;126:193–215. [PubMed: 11105648]

Jeong M, Tashiro M, Singh LN, Yamaguchi K, Horikawa E, Miyake M, Watanuki S, Iwata R, Fukuda H, Takahashi Y, et al. Functional brain mapping of actual car-driving using [18F]FDG-PET. Ann Nucl Med 2006;20:623–628. [PubMed: 17294673]

Kamimura N, Kakeda K, Kitamura Y, Sanada J, Ikeda M, Inoue S. Dementia and driving: present status of drivers with dementia and response of their family's care in Japan. No To Shinkei 2005;57:409–414. [PubMed: 15981640]

Kapur, BM. Computer Blood Alcohol Calculator v1.20 ARF Software. Toronto, Canada: Addiction Research Foundation; 1989.

Krull KR, Smith LT, Sinha R, Parsons OA. Simple reaction time event-related potentials: Effects of alcohol and sleep deprivation. Alcohol Clin Exp Res 1993;17:771–777. [PubMed: 8214412]

Lamb MR, Robertson LC. Effect of acute alcohol on attention and the processing of hierarchical patterns. Alcohol Clin Exp Res 1987;11:243–248. [PubMed: 3307487]

Lancaster JL, Woldorff MG, Parsons LM, Liotti M, Freitas CS, Rainey L, Kochunov PV, Nickerson D, Mikiten SA, Fox PT. Automated Talairach atlas labels for functional brain mapping. Hum Brain Mapp 2000;10:120–131. [PubMed: 10912591]

Levin JM, Ross MH, Mendelson JH, Kaufman MJ, Lange N, Maas LC, Mello NK, Cohen BM, Renshaw PF. Reduction in BOLD fMRI response to primary visual stimulation following alcohol ingestion. Psychiatry Res 1998;82:135–146. [PubMed: 9754438]

Levy R, Czernecki V. Apathy and the basal ganglia. J Neurol 2006;253(Suppl 7):VII54–VII61. [PubMed: 17131230]

Li, Yo; Adali, T.; Calhoun, VD. Estimating the number of independent components for functional magnetic resonance imaging data. Hum Brain Mapp. 2007

Linnoila M, Mattila MJ. Interaction of alcohol and drugs on psychomotor skills as demonstrated by a driving simulator. Br J Pharmacol 1973;47:671P–672P.

Moskowitz H, Sharma S. Effects of alcohol on peripheral vision as a function of attention. Hum Factors 1974;16:174–180. [PubMed: 4844761]

Oscar-Berman M, Marinković K. Alcohol: Effects on neuro-behavioral functions and the brain. Neuropsychol Rev 2007;17:239–257. [PubMed: 17874302]

Paulus MP, Tapert SF, Pulido C, Schuckit MA. Alcohol attenuates load-related activation during a working memory task: Relation to level of response to alcohol. Alcohol Clin Exp Res 2006;30:1363–1371. [PubMed: 16899039]

Raichle ME, MacLeod AM, Snyder AZ, Powers WJ, Gusnard DA, Shulman GL. A default mode of brain function. Proc Natl Acad Sci USA 2001;98:676–682. [PubMed: 11209064]

Rimm DC, Sininger RA, Faherty JD, Whitley MD, Perl MB. A balanced placebo investigation of the effects of alcohol vs. alcohol expectancy on simulated driving behavior. Addict Behav 1982;7:27–32. [PubMed: 7080881]

Rosen LJ, Lee CL. Acute and chronic effects of alcohol use on organizational processes in memory. J Abnorm Psychol 1976;85:309–317. [PubMed: 945308]

Seifritz E, Bilecen D, Hänggi D, Haselhorst R, Radü EW, Wetzel S, Seelig J, Scheffler K. Effect of ethanol on BOLD response to acoustic stimulation: Implications for neuropharmacological fMRI. Psychiatry Res 2000;99:1–13. [PubMed: 10891645]

Spiers HJ, Maguire EA. Neural substrates of driving behaviour. Neuroimage 2007;36:245–255. [PubMed: 17412611]

Talairach, J.; Tournoux, P. Co-planar Stereotactic Atlas of the Human Brain. 3-Dimensional Proportional system — an Approach to Cerebral Imaging. New York, NY: Thieme Medical Publishers; 1988.

Tarter RE, Arria AM, Van Thiel DH. Hepatic encephalopathy coexistent with alcoholism. Recent Dev Alcohol 1991;9:205–224. [PubMed: 1758984]

Uchiyama Y, Ebe K, Kozato A, Okada T, Sadato N. The neural substrates of driving at a safe distance: a functional MRI study. Neurosci Lett 2003;352:199–202. [PubMed: 14625019]

Verster JC, Volkerts ER, Verbaten MN. Effects of alprazolam on driving ability, memory functioning and psychomotor performance: A randomized, placebo-controlled study. Neuropsychopharmacology 2002;27:260–269. [PubMed: 12093599]

Walter H, Vetter SC, Grothe J, Wunderlich AP, Hahn S, Spitzer M. The neural correlates of driving. Neuroreport 2001;12:1763–1767. [PubMed: 11409755]

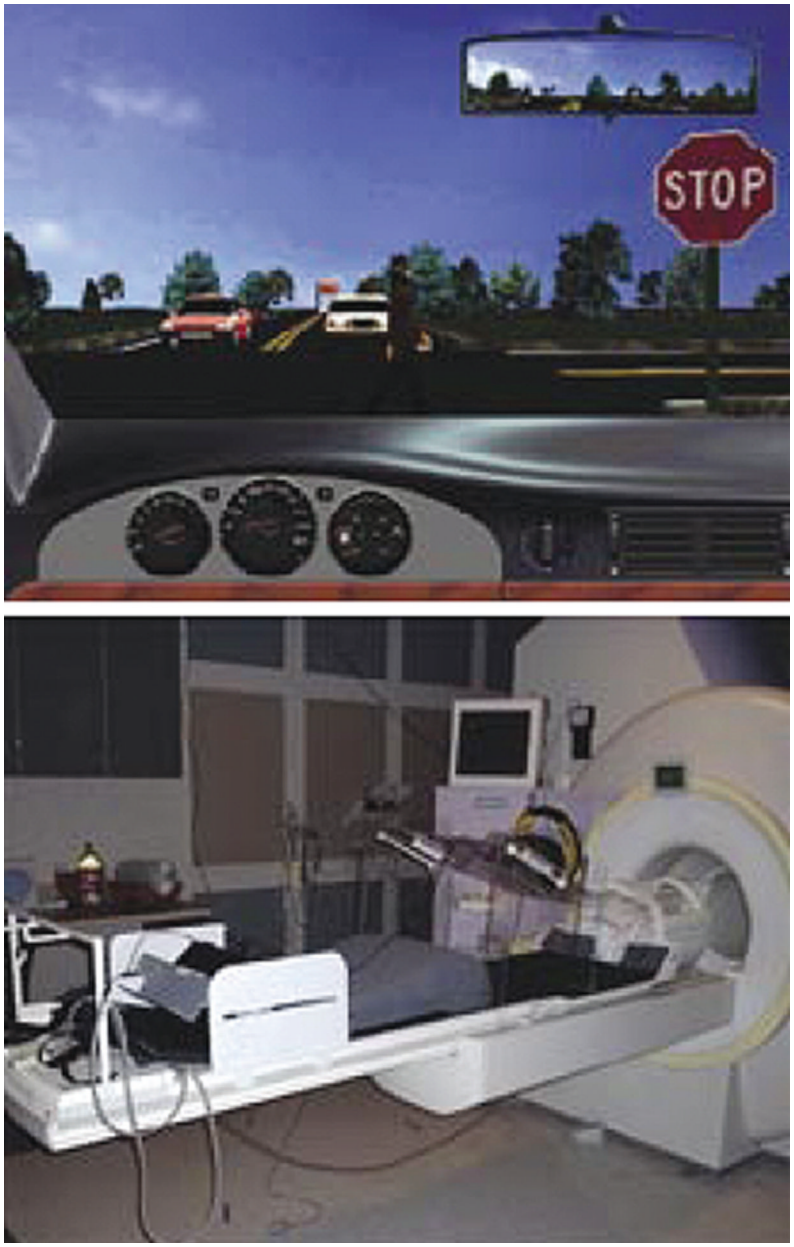

Figure 1.
In scanner driving setup and snapshot of a virtual driving scenario. A screen shot from the driving simulator and scanner driving setup.

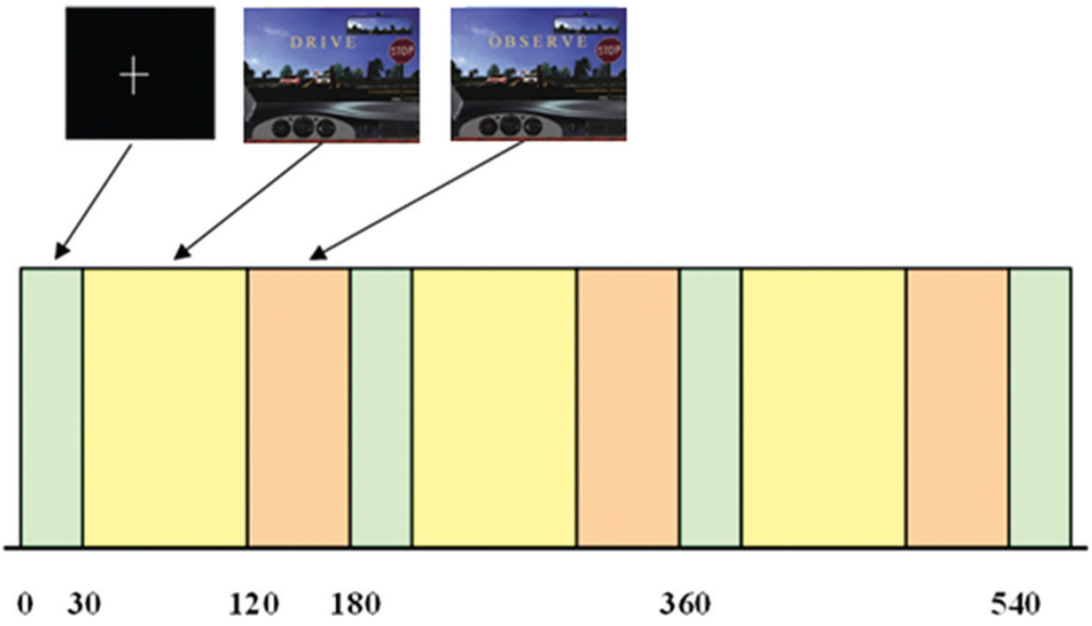

Figure 2.
Driving paradigm design. Functional driving paradigm with a block design having the following phases: Fixate, 30 s, Drive, 90 s, and Observe, 60 s.

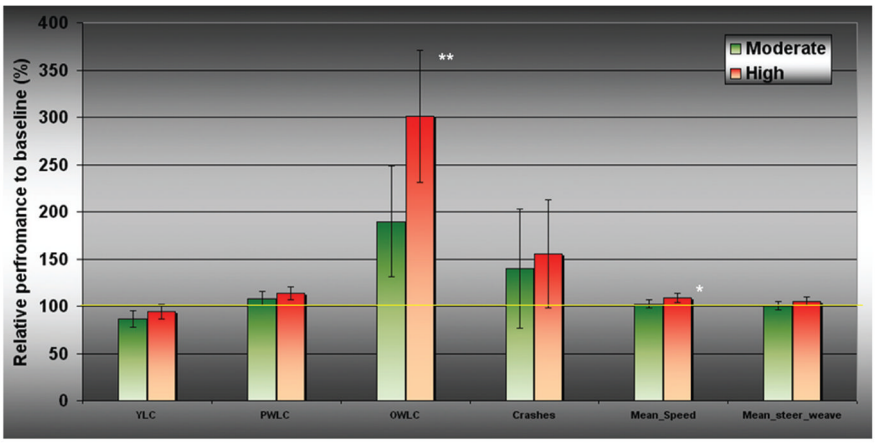

Figure 3.

Dose-related driving behavior scores. Behavior results from the driving data. Driving performance at moderate- and high-dose EtOH (green and red bars respectively) compared to (mean) placebo performance (solid yellow line) rated on six different measures. Measured yellow line crossing (YLC), passenger white line crossing (PWLC), opposite white line crossing (OWLC), crashes, mean speed, and mean steering weave (*Significant at $P < 0.05$; **Significant at $P < 0.01$).

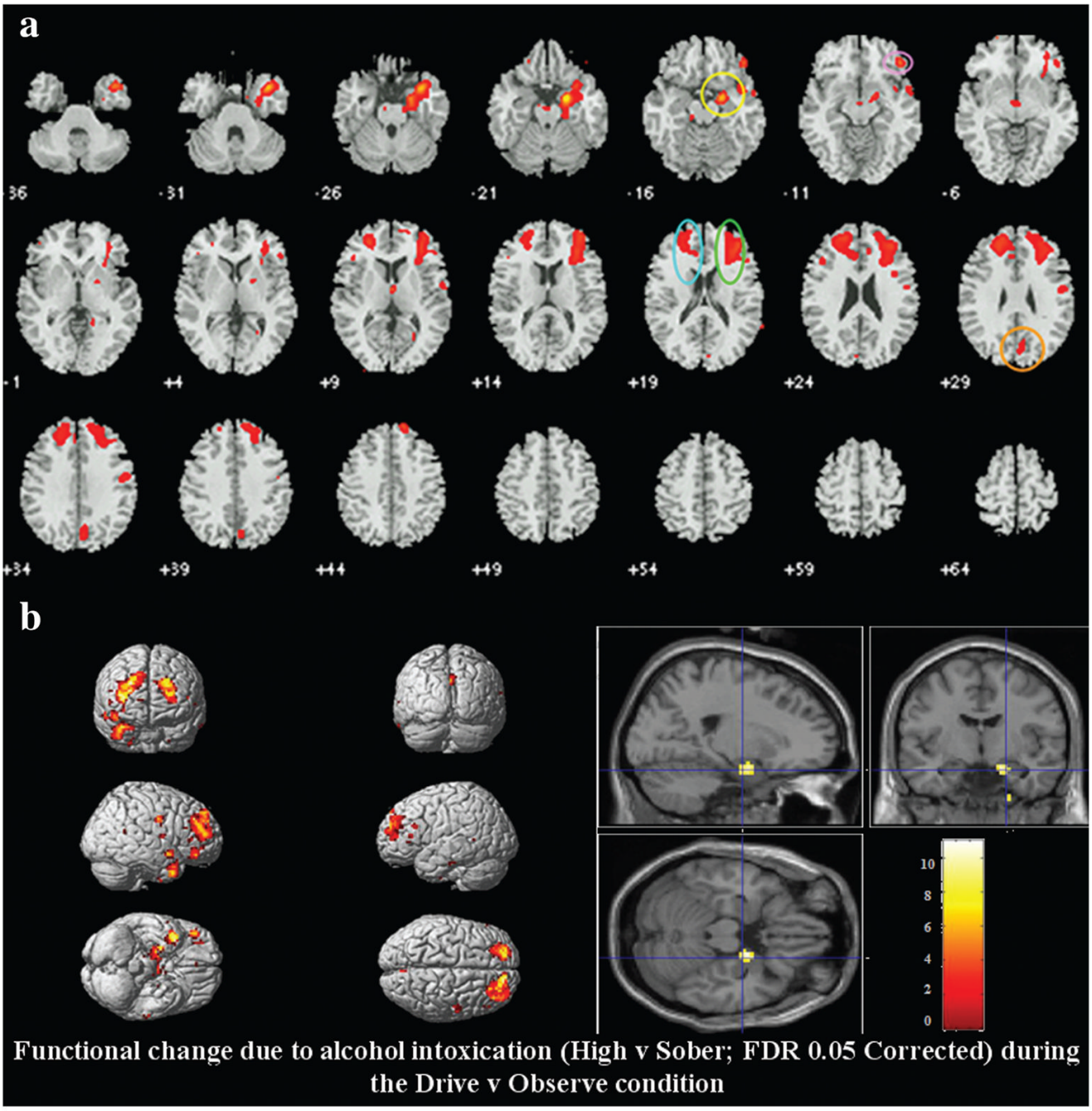

Figure 4.

GLM analysis. Functional changes due to alcohol intoxication. **a** (top): Regions that demonstrated a significantly lower functional activation (drive vs. observe) during the high dose relative to placebo condition (thresholded at $P = 0.05$ FDR corrected). Maps were derived from a random effects (RFX) repeated measures analysis comparing the two dosages conducted through a standard GLM analysis in SPM2. **b** (below): Areas of activation (high vs. sober; $P < 0.05$ FDR corrected) during the drive-observe condition shown on a rendered brain along with an orthogonal display of slices depicting a significant dose-related functional change in the amygdala/parahippocampus region. (Note: Color bar shown corresponds to both the overall and amygdala/parahippocampus activation patterns).

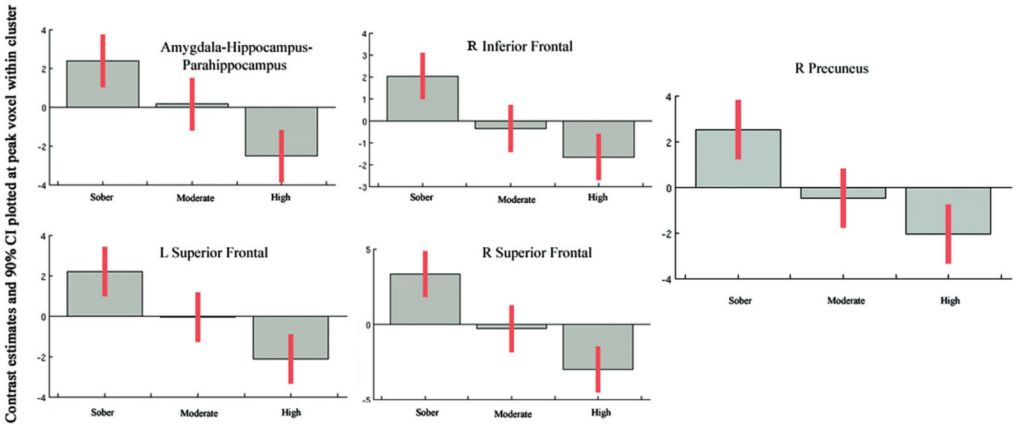

Figure 5.

Dose-related responses plotted across five major regions revealed by GLM. Effect sizes of functional responses at peak voxel within each major cluster identified by RFX analysis. Note the linear pattern of signal change observed across dosage. *X*-axis refers to dosage condition and *Y*-axis refers to mean signal difference.

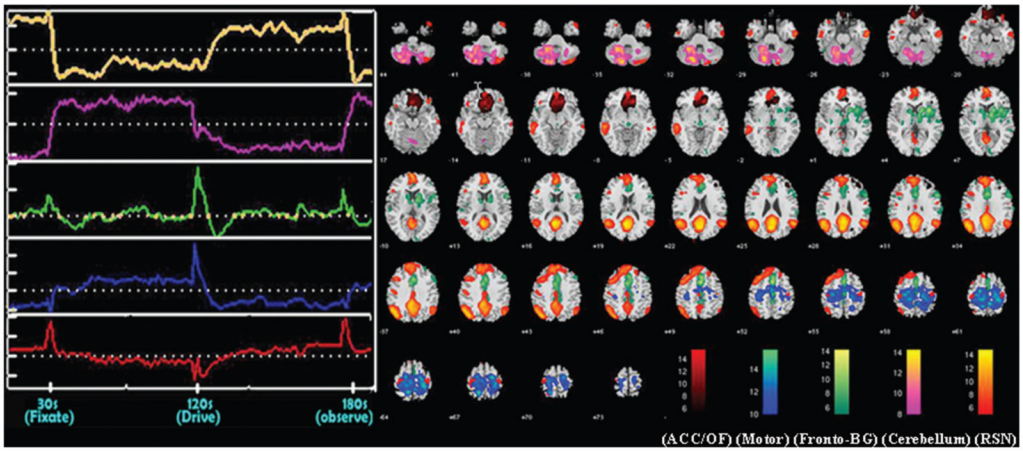

Figure 6.

ICA networks and associated time courses that differed significantly across alcohol doses. RFX group maps thresholded at $P = 0.05$ FDR corrected and associated time courses of brain circuits that demonstrated a significant alcohol-related fMRI difference. Spatial maps correspond to mean response over all three doses. Normalized time course signal is depicted in relation to a "zero" baseline (dotted line). A total of five components are presented. The OF and anterior cingulate areas are depicted in red. Cerebellar and Motor areas are depicted in pink and blue respectively. The frontal-basal-temporal component is shown in green. An "orange" component extending across the medial frontal, bilateral parietal, and cingulate regions represents the "idling condition" or resting state network (RSN) of the brain.

TABLE I

Significant regions (drive vs. observe condition) showing decreased activation during the high dose relative to the placebo dose (0.05 FDR corrected), as identified using a GLM analysis, along with their MNI coordinates and maximum *T* values

Regions	Brodmann area	Left (Vol CC)	Left Max *T* (MNI co-ordinates)	Right (Vol CC)	Right Max *T* (MNI co-ordinates)
Superior frontal gyrus	10, 9, 8	3.5	3.6 (−21, 52, 15)	4.4	3.6 (15, 54, 30)
Middle frontal gyrus	10, 6, 46	1	3.7 (−24, 52, 15)	2.5	4 (36, 52, 3)
Precuneus	7, 31	0.2	3.4 (−3, −57, 33)	1.4	3.6 (0, −57, 33)
Parahippocampal gyrus	34, Amygdala, Hippocampus, 28	0	NS	0.9	3.8 (18, −10, −14)
Inferior frontal gyrus	10, 46, 47	0.3	3.4 (−48, 33, 9)	0.4	3.8 (39, 48, −2)
Medial frontal gyrus	9	0.6	3.5 (−24, 43, 3)	0.1	3.5 (12, 57, 2)
Superior temporal gyrus	38	<0.1	3.4 (−30, 10, −18)	0.4	3.7 (36, 9, −22)
Uncus	Amygdala, 28	<0.1	3.4 (−30, 7, −18)	0.3	3.6 (24, −2, −17)
Cingulate gyrus	31	0	NS	0.2	3.4 (3, −57, 29)
Cuneus	7	0	NS	0.1	3.4 (0, −62, 32)
Precentral gyrus	6, 4	0	NS	0.1	3.3 (61, 2, 13)
Anterior cingulate	9, 32	0.1	3.3 (−21, 38, 12)	0	NS

TABLE II

ICA component regions that showed a significant dose-related change along with their MNI coordinates and corresponding Talairach labels

Regions	Hypothesized functionality	Brod-mann Area	Left (Vol CC)	Right (Vol CC)	Total (Vol CC)	Left Max *T* (MNI coords)	Right Max *T* (MNI coords)	Overall dosage related significance (*P* value)	Similar component from Calhoun et al., 2004a
RED COMPONENT	Error Monitoring and inhibition							0.04	Pink Component*
Anterior Cingulate		10, 32, 24, 25	3.2	3.2	6.4	11.9 (−6, 35, −9)	14.4 (12, 33, −6)		
Medial Frontal/Orbital Gyrus		10, 11, 25	3.9	3.6	7.5	12.6 (−3, 30, −15)	15.2 (12, 36, −6)		
Superior Frontal Gyrus		11, 10, 9, 6	0.5	1.8	2.3	6.7 (−12, 54, −18)	7.6 (12, 48, −15)		
Inferior Frontal Gyrus		47, 11, 46	0.3	2	2.3	8.3 (−12, 39, −24)	8.5 (15, 23, −18)		
Middle Frontal Gyrus		10, 46, 11, 9	0.1	2.6	2.7	7.3 (−15, 42, −24)	8.5 (39, 39, 24)		
Rectal Gyrus		11	1	0.7	1.7	11.7 (−6, 30, −21)	8.8 (3, 27, −21)		
Subcallosal Gyrus		25, 11, 47	1.3	1.4	2.7	10.9 (−9, 15, −12)	12.6 (6, 18, −14)		
BLUE COMPONENT	Gross/Fine Motor Control							0.02	Red Component*
Postcentral Gyrus		7, 5, 3, 2, 40, 1	11.6	14	25.6	15.6 (−12, −51, 66)	14.7 (27, −36, 63)		
Precentral Gyrus		4, 6	11	14.3	25.3	14.4 (−21, −24, 72)	14.4 (27, −33, 62)		
Medial Frontal Gyrus		6, 32, 10	9.9	9.1	19	13.7 (−9, −27, 63)	13.2 (0, −9, 54)		
Cingulate Gyrus		24, 31, 32	7	7.3	14.3	14.2 (−3, −6, 51)	13.8 (0, −9, 51)		
Precuneus		7	6.8	4.9	11.7	15.5 (−9, −51, 63)	13.1 (9, −48, 59)		
Paracentral Lobule		5, 6, 3, 4, 31, 7	5.5	5.8	11.3	14.4 (−12, −33, 60)	15.3 (6, −42, 60)		
Superior Frontal Gyrus		6, 8	5.6	5.7	11.3	13.1 (−9, −21, 69)	14.8 (21, −12, 69)		

Regions	Hypothesized functionality	Brod-mann Area	Left (Vol CC)	Right (Vol CC)	Total (Vol CC)	Left Max *T* (MNI coords)	Right Max *T* (MNI coords)	Overall dosage related significance (*P* value)	Similar component from Calhoun et al., 2004a
Middle Frontal Gyrus		6, 10, 8	5	5.7	10.7	14.6 (−18, −12, 62)	14.8 (18, −14, 66)		
Inferior Parietal Lobule		40, 2	2.5	2.9	5.4	11.1 (−30, −42, 60)	12.4 (33, −42, 60)		
Superior Parietal Lobule		7, 5	2.3	2.9	5.2	11.6 (−18, −54, 64)	11.9 (18, −51, 60)		
S									
GREEN COMPONENT	Motor planning, Goal directedness							0.05	Not Observed
Cingulate Gyrus		24, 32, 31	4.6	6.8	11.4	12.1 (−6, 6, 40)	11.3 (0, 18, 36)		
Sub Nuclei		Putamen Lateral, Globus, Pallidus, 47	3.1	7.8	10.9	9.1 (−9, −3, 12)	11.5 (9, 0, 7)		
Middle Frontal Gyrus		9, 8, 6, 46	0.7	3.9	4.6	6.5 (−42, 0, 42)	9.7 (51, 12, 33)		
Medial Frontal Gyrus		6, 8, 32, 9	2.6	4.8	7.4	11.7 (−3, 12, 51)	12.5 (0, 9, 51)		
Superior Frontal Gyrus		6, 8, 9, 10	1.3	2.9	4.2	9.8 (−3, 12, 54)	11.5 (0, 12, 54)		
Inferior Frontal Gyrus		9, 44, 47, 45, 46	0.6	3.4	4	6.5 (−42, 6, 30)	10.6 (54, 12, 30)		
Superior Temporal Gyrus		22, 42, 41, 38, 21	0.8	2.2	3	6.6 (−51, 15, −12)	7.6 (60, −16, 0)		
Insula		13, 47	1	3.8	4.8	7 (−36, 9, 6)	12.1 (33, 12, 6)		
Anterior Cingulate		32, 24, 33, 42	1.6	2.8	4.4	7.7 (−3, 36, 27)	9.4 (0, 39, 24)		
Thalamus		Ventral, Anterior, NucleusVentral	1	2	3	8.4 (−9, −6, 10)	10.9 (9, −3, 6)		
Caudate		Caudate, HeadCaudate, Body	1.2	1.4	2.6	8.4 (−12, 12, 9)	11.1 (15, 15, 6)		
Paracentral Lobule		31, 5, 6	0.6	1.7	2.3	7.5 (−3, −39, 51)	9.5 (0, −39, 51)		
Inferior Parietal Lobule		40	0.8	1.3	2.1	6.9 (−48, −33, 27)	7.6 (60, −30, 27)		

Regions	Hypothesized functionality	Brod-mann Area	Left (Vol CC)	Right (Vol CC)	Total (Vol CC)	Left Max *T* (MNI coords)	Right Max *T* (MNI coords)	Overall dosage related significance (*P* value)	Similar component from Calhoun et al., 2004a
Precentral Gyrus		44, 9, 6	0.2	1.5	1.7	5.8 (−57, 9, 9)	10 (54, 9, 12)		
Cuneus		17, 18	0	1.6	1.6	NS	7.6 (6, −96, 9)		
Lingual Gyrus		17, 18	0.1	1	1.1	5.7 (−3, −90, −12)	7.2 (12, −87, −12)		
PINK COMPONENT	Fine Motor Control							0.03	Orange-Turquoise
Cerebellum		Declive, Cerebellar Tonsil, Inferior Semi-Lunar Lobule, Culmen, Pyramis	33	18	51	14.3 (−21, −72, −30)	11.4 (12, −69, −24)		
Middle Frontal Gyrus		9, 46, 10, 8, 6	0	2.1	2.1	NS	9.1 (54, 27, 40)		
Precentral Gyrus		6, 4	0	1.3	1.3	NS	7.2 (30, −24, 51)		
ORANGE COMPONENT	Baseline condition							0.03	Blue Component
Posterior Cingulate		23, 30, 31, 29	5.7	3.8	9.5	14.8 (−6, −60, 18)	13.6 (0, −57, 18)		
Precuneus		31, 23, 19, 7, 39, 18	11.5	9.4	20.9	14.2 (−6, −63, 18)	14.1 (3, −66, 20)		
Cingulate Gyrus		31, 23, 24, 32	6.2	5.4	11.6	14 (−3, −54, 27)	14.1 (0, −54, 27)		
Cuneus		7, 30, 18, 19	1.6	0.6	2.2	14 (−3, −72, 30)	12.5 (0, −72, 30)		
Angular Gyrus		39	2.7	1.2	3.9	13.9 (−48, −63, 36)	8.7 (51, −63, 30)		
Inferior Parietal Lobule		39, 40, 7	6.3	2.8	9.1	13.8 (−42, −72, 39)	10.2 (48, −69, 39)		
Superior Temporal Gyrus		39, 38, 22	3.8	1.7	5.5	13.3 (−51, −57, 24)	12.2 (57, −60, 24)		
Supramarginal Gyrus		40, 39	4.4	3.9	8.3	13.3 (−51, −60, 33)	12.1 (51, −57, 27)		
Medial Frontal Gyrus		10, 8, 9, 6, 32, 11	10.2	5.4	15.6	12.6 (−6, 63, 9)	11.8 (3, 48, 45)		

Regions	Hypothesized functionality	Brod-mann Area	Left (Vol CC)	Right (Vol CC)	Total (Vol CC)	Left Max *T* (MNI coords)	Right Max *T* (MNI coords)	Overall dosage related significance (*P* value)	Similar component from Calhoun et al., 2004a
Middle Temporal Gyrus		39, 21, 19, 20, 22, 38, 37	9.1	2.4	11.5	12.3 (−48, −60, 24)	9.2 (51, −63, 27)		
Superior Parietal Lobule		7	1.1	0	1.1	12.1 (−36, −75, 45)	NS		
Superior Frontal Gyrus		9, 8, 10, 6	13.3	3.4	16.7	11.2 (−12, 57, 24)	9.8 (3, 51, 39)		
Inferior Temporal Gyrus		20, 21	1.2	1.8	3	8.7 (−54, −6, −27)	11.1 (57, −12, −27)		
Middle Frontal Gyrus		8, 9, 6, 11, 10, 46	8.2	0.5	8.7	11 (−45, 12, 49)	8.7 (39, 36, −15)		
Anterior Cingulate		42, 32, 10	2.4	0.5	2.9	10.7 (−6, 45, 15)	9.5 (3, 48, 12)		
Precentral Gyrus		9, 4, 6	4.4	2.1	6.5	9.9 (−42, 21, 39)	8 (54, −6, 30)		
Inferior Frontal Gyrus		47, 45, 11, 9	2.1	0.2	2.3	7.7 (−30, 21, −21)	8.3 (36, 36, −18)		
Postcentral Gyrus		3, 2, 7	0.9	0.5	1.4	7.4 (−42, −27, 60)	6.3 (45, −18, 57)		

TABLE III

Principal-component analysis for six driving behavioral measures

	Rotated Components	
	1	**2**
Eigenvalues	1.911	1.852
Variance	31.848	30.872
Component Loading		
Yellow Line Crossings	0.055	**0.779**
Passenger White Line Crossings	**0.755**	−0.186
Opposite White Line Crossings	−0.014	**0.710**
Crashes	0.024	**0.819**
Mean Speed	**0.772**	0.178
Mean Steering Weave	**0.861**	0.071

Component loadings of 0.6 or higher were considered significant and are in bold.